A&A 480, L5–L8 (2008)
DOI: 10.1051/0004-6361:20079296


Astronomy & Astrophysics

Letter to the Editor

# CN in prestellar cores⋆,⋆⋆

P. Hily-Blant[1,⋆⋆⋆], M. Walmsley[2], G. Pineau des Forêts[3,4], and D. Flower[5]

[1] IRAM, Domaine Universitaire, 300 rue de la Piscine, 38406 Saint-Martin d'Hères, France
e-mail: hilyblan@iram.fr
[2] INAF – Osservatorio Astrofisico di Arcetri, Largo Enrico Fermi 5, 50125 Firenze, Italy
[3] IAS (UMR 8617 du CNRS), Université de Paris-Sud, 91405 Orsay, France
[4] LERMA (UMR 8112 du CNRS), Observatoire de Paris, 61 avenue de l'Observatoire, 75014 Paris, France
[5] Physics Department, The University, Durham DH1 3LE, UK

Received 20 December 2007 / Accepted 15 January 2008

**ABSTRACT**

*Context.* Determining the structure of and the velocity field in prestellar cores is essential to understanding protostellar evolution.
*Aims.* We have observed the dense prestellar cores L 1544 and L 183 in the $N = 1 \rightarrow 0$ rotational transition of CN and $^{13}$CN in order to test whether CN is depleted in the high-density nuclei of these cores.
*Methods.* We have used the IRAM 30 m telescope to observe along the major and minor axes of these cores. We compare these observations with the 1 mm dust emission, which serves as a proxy for the hydrogen column density.
*Results.* We find that while CN(1−0) is optically thick, the distribution of $^{13}$CN(1−0) intensity follows the dust emission well, implying that the CN abundance does not vary greatly with density. We derive an abundance ratio of $[CN]/[H_2] = 10^{-9}$ in L 183 and $1-3 \times 10^{-9}$ in L 1544, which, in the case of L 183, is similar to previous estimates obtained by sampling lower-density regions of the core.
*Conclusions.* We conclude that CN is not depleted towards the high-density peaks of these cores and thus behaves like the N-containing molecules $N_2H^+$ and $NH_3$. CN is, to our knowledge, the first C-containing molecule to exhibit this characteristic.

**Key words.** ISM: abundances – ISM: individual objects: L 1544 – ISM: individual objects: L 183

## 1. Introduction

Knowledge of the structure and kinematics of prestellar cores is important to our understanding of protostellar evolution. Cores which are close to the critical point at which collapse sets in are representative of the preliminary phase of evolution which subsequently leads to the formation of a protostar. In this context, the cores with the highest central density and/or column density are the most interesting; but the fact that CO and many other tracers of the kinematics deplete on to dust grain surfaces at densities above $10^5$ cm$^{-3}$ (Tafalla et al. 2002) has been an obstacle to progress in this area. Fortunately, observations have suggested that some N-containing species, such as $NH_3$ and $N_2H^+$, remain in the gas phase at densities above $10^5$ cm$^{-3}$. Given that both $NH_3$ and $N_2H^+$ form from $N_2$ and that the volatility of $N_2$ is similar to that of CO (Öberg et al. 2005), it is puzzling that even these species survive. There is some evidence that they finally freeze out at densities $\gtrsim 10^6$ cm$^{-3}$ (Bergin et al. 2002; Belloche & André 2004; Pagani et al. 2007), and, irrespective of the reason for this behaviour, it would be useful to find other tracers of the densest gas in the cores.

Radicals represent a type of "molecule" which tends to resist depletion; this comes about because, typically, they are both formed and destroyed by neutral-neutral substitution reactions in which both formation and destruction depend in the same manner on the abundance of an atom, such as C, N, or O. An example is NO, which is believed to be formed and destroyed by reactions with atomic nitrogen. Under these conditions, the fractional abundance of NO is independent of the degree of depletion of atomic N. In a previous article (Akyilmaz et al. 2007, hereafter A07), we attempted to test this hypothesis by observing NO in two high density cores. We found, to our discomfiture, that the hypothesis was incorrect: NO becomes depleted in the high density cores of L 1544 and L 183 similarly to many other species. The explanation of this observational result is not entirely clear, but it probably has to do with the fraction of oxygen which remains in the gas phase at high densities.

The motivation for our NO study arose partly from the issues of the nitrogen chemistry, referred to earlier. NO has been considered to be the main intermediary between atomic and molecular nitrogen, which are probably the main forms of elemental nitrogen in the gas phase in molecular clouds. However, the fact that NO appears to be not present in the densest gas suggested that there may be other intermediaries between N and $N_2$ and that a possible candidate might be CN. CN can form from hydrocarbons, such as CH, in reactions with atomic N (Pineau des Forêts et al. 1990) and is destroyed, also by N, forming $N_2$. Thus, if elemental carbon is present in the dense gas, CN might mediate in the formation of $N_2$ and hence in the formation of $NH_3$ and $N_2H^+$. However, the fraction of elemental carbon which is available to form hydrocarbons in the dense regions of prestellar cores is uncertain. The reason for this uncertainty is that the main reservoir of carbon in the gas phase

⋆ Based on observations carried out with the IRAM-30 m telescope. IRAM is supported by INSU-CNRS/MPG/IGN.
⋆⋆ Appendices are only available in electronic form at http://www.aanda.org
⋆⋆⋆ Currently at LAOG (UMR 5571) Observatoire de Grenoble.

of molecular clouds is CO, and if CO freezes out, it might be expected that there remains little carbon to form hydrocarbons and, by extension, CN. However, from an observational point of view, one knows only that CO is at least an order of magnitude underabundant in prestellar core nuclei. There are non-thermal processes (e.g. Leger et al. 1985) which can maintain gas phase CO at abundances of order $[CO]/[H_2] = 10^{-6}$ at densities of order $10^6$ cm$^{-3}$ and which might suffice to produce appreciable amounts of $C^+$, a precursor of CH, following the reaction of CO with cosmic-ray produced $He^+$.

The present Letter presents observations of CN and $^{13}$CN which demonstrate that CN is relatively abundant in the high density cores of L 183 and L 1544. In Sect. 2, we summarize the observations and, in Sect. 3, we present the basic observational results. Section 4 contains a brief discussion of the implications of our observational results for chemical models.

## 2. $^{12}$CN and $^{13}$CN(1–0) observations

Observations were carried out with the IRAM 30 m telescope. The CN($N = 1 \rightarrow 0, F_2 = 3/2 \rightarrow 1/2$) multiplet (113.5 GHz: see Table B.1) was observed at different epochs between December 2006 and August 2007, under average to good weather conditions. Observations of the $^{13}$CN($N = 1 \rightarrow 0, F_2 = 2 \rightarrow 1$) multiplet (at 108.8 GHz Gerin et al. 1984) were performed in August 2007 under good conditions. The HPBW at the CN and $^{13}$CN frequencies are 22″ and 22.8″, respectively. The VESPA facility autocorrelator was used to obtain 20 kHz channel spacing, with 60 MHz and 35 MHz bandwidths for CN and $^{13}$CN, respectively. Hence we cover the five strongest hyperfine structure (HFS) transitions of both isotopologues. The observing strategy was identical for all measurements: frequency-switching mode with a 7.8 MHz throw and a phase time of 0.5 s, with atmospheric and bandpass amplitude calibrations every 10 to 15 min. Data reduction and analysis were completed using the CLASS software (Hily-Blant et al. 2005) of the GILDAS facility (Pety 2005). Instrumental bandpass and atmospheric contributions were subtracted with polynomial baselines, before and after the folding of the two-phase spectra. Concerning the CN spectra, the SSB receiver and system temperatures were $T_{\rm rec} = 75$ K and $T_{\rm sys} \approx 170$ K, with zenith opacity 0.13. The final rms, in the main-beam temperature ($T_{\rm mb}$), in each channel of width $\delta v = 0.052$ km s$^{-1}$ is $\sigma_{\rm T} \approx 70$ mK for both L 1544 and L 183. Regarding $^{13}$CN, $T_{\rm rec} = 70$–$90$ K and $T_{\rm sys} = 100$–$250$ K, resulting in signal band zenith opacities 0.05–0.1. The final rms in each channel of width $\delta v = 0.054$ km s$^{-1}$ are $\sigma_{\rm T} \approx 15$ mK towards L 1544, and 17 mK towards L 183. In what follows, all temperatures are on the main-beam scale, $T_{\rm mb} = F_{\rm eff} T_{\rm A}^* / B_{\rm eff}$ where $T_{\rm A}^*$ is the antenna temperature corrected for atmospheric absorption, and the forward and beam efficiencies are respectively $F_{\rm eff} = 0.95$ and $B_{\rm eff} = 0.75$.

The observations were made along two cuts, following the major and minor axes of L 1544 and L 183: see Fig. 1.

## 3. Results

### 3.1. $^{12}$CN

In Fig. 2, we show our CN($N = 1 \rightarrow 0, F_2 = 3/2 \rightarrow 1/2$) spectra towards the (0, 0) positions in L 183 and L 1544. It is noteworthy that the L 1544 profiles are double-peaked (see Fig. C.1) and, more significantly, that the observed intensity ratios of the HFS components in both sources are inconsistent with the values expected under optically thin LTE conditions; we list the expected and observed ratios in Table B.1. In L 183, the transition of highest intrinsic strength, at 113 490.985 MHz, is far from being the most intense line observed. The most likely explanation is that the lines are optically thick. Accordingly, we decided to observe the corresponding $^{13}$CN lines. It is striking that the $^{12}$CN lines peak in roughly the same position as the dust millimeter emission; this is apparent in Fig. 3, where we plot the integrated intensity of the (intrinsically weakest and hence most likely to be optically thin) $F \rightarrow F' = 1/2 \rightarrow 3/2$ line at 113 520.34 MHz against offset from (0, 0). One sees that, at least in L 1544, the line intensity is highest not far from the peak in the dust emission, suggesting that the CN column density is a maximum at that position.

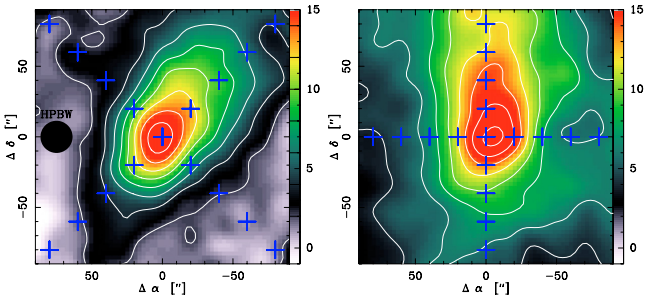


**Fig. 1.** Dust emission at 1.3 mm (in MJy sr$^{-1}$) towards L 1544 (*left*) and L 183 (*right*) from Ward-Thompson et al. (1999) and Pagani et al. (2004), respectively. The crosses indicate the positions where the $^{13}$CN(1–0) emission was measured (North is to the top). In L 1544, the NE–SW and NW–SE cuts are referred to as the minor and major axes, respectively. In L 183, major and minor refer to N–S and E–W, respectively. The 22.8″ HPBW at 108.8 GHz is indicated. The (0, 0) position corresponds to $\alpha(2000) = 05^{\rm h}04^{\rm m}16.9^{\rm s}$, $\delta(2000) = 25°10'47''$ for L 1544 and $\alpha(2000) = 15^{\rm h}54^{\rm m}08.8^{\rm s}$, $\delta(2000) = -02°52'44''$ for L 183.

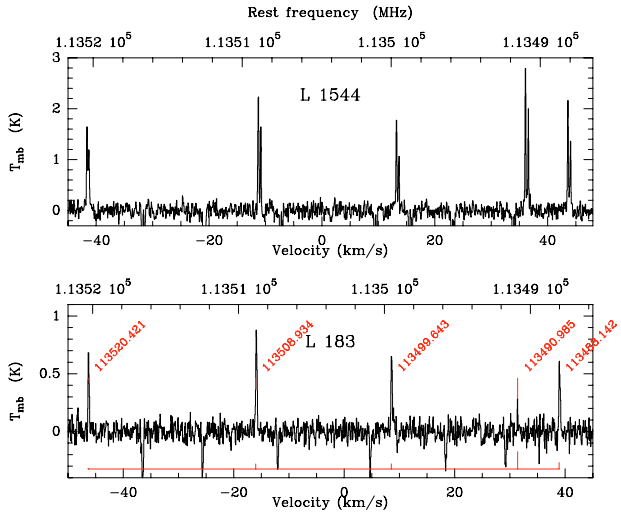


**Fig. 2.** CN($N = 1 \rightarrow 0, F_2 = 3/2 \rightarrow 1/2$) spectrum towards the (0, 0) positions in L 1544 (*top*) and L 183 (*bottom*). The relative line intensities expected under optically thin LTE conditions are shown towards the bottom of the lower panel.

### 3.2. $^{13}$CN

Figure 4 shows the (0, 0) $^{13}$CN($N = 1 \rightarrow 0, F_2 = 2 \rightarrow 1$) spectrum towards the two cores. In both cores, the emission in the main $F = 3 \rightarrow 2$ 108 780.201 MHz component was successfully detected at all offsets smaller than 40″. Towards L 183,

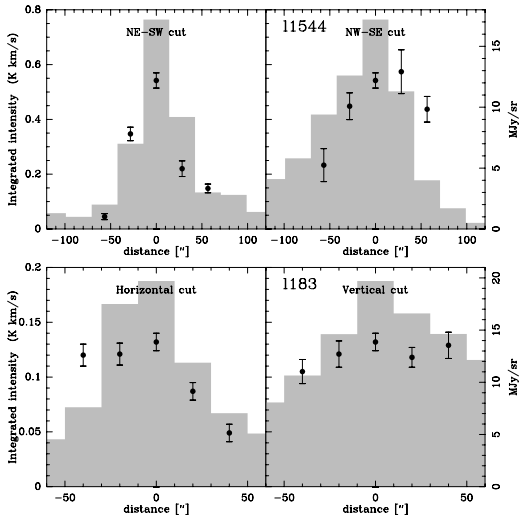


**Fig. 3.** Cuts of the integrated intensity (K km s$^{-1}$) (*left hand scale*) of the weakest HFS component of CN($N = 1 \rightarrow 0, F_2 = 3/2 \rightarrow 1/2$), at rest frequency 113 520.4 MHz and with relative intensity 0.0123, towards L 1544 (*top*) and L 183 (*bottom*). The light histogram is the dust emission, in MJy sr$^{-1}$ (*right hand scale*).

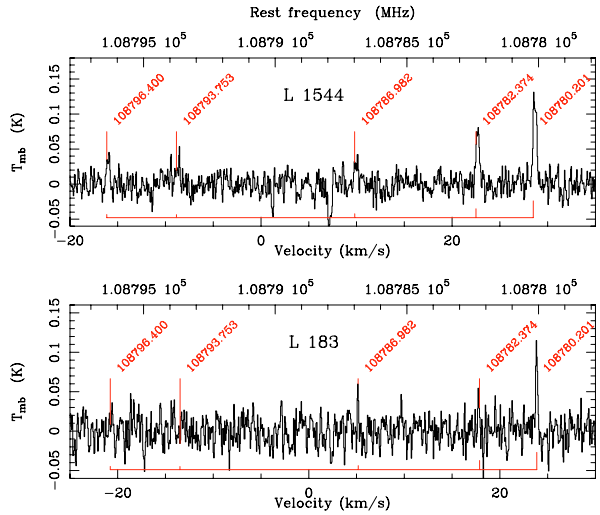


**Fig. 4.** $^{13}$CN($N = 1 \rightarrow 0, F_2 = 2 \rightarrow 1$) spectrum at positions (0, 0) in L 1544 (*top*) and L 183 (*bottom*). The five observed HFS components are indicated.

we detect only the main HFS component at most positions, although the $F = 2 \rightarrow 1$ transition at 108 782.37 MHz is seen also at offset (20, 0). Towards L 1544, we detect several components and can determine their relative intensities. At each position, a Gaussian profile was fitted to the main component (with relative intensity $R = 0.194$) from which we obtain the integrated intensity, $W_{\rm main}$ (on the $T_{\rm mb}$ scale). At some positions toward L 1544, the lines are double-peaked (Williams et al. 1999; van der Tak et al. 2005), in which case a two-component Gaussian fit was made. The line parameters are given in Tables 1 and 2.

We note that the intensity ratios of the HFS components are consistent with low optical depths, which we have assumed when estimating the CN column density. We assume also that the level populations are consistent with LTE at a temperature of 8 K (a compromise between estimates quoted in the literature, e.g. Crapsi et al. 2007; Pagani et al. 2007). For the [$^{12}$CN]/[$^{13}$CN] abundance ratio, we adopt a value of 68 (Milam et al. 2005).

**Table 1.** $^{13}$CN column density in L 1544, $N(^{13}{\rm CN})$ (in units of $10^{12}$ cm$^{-2}$), with $W = W_{\rm main}/R$ (in mK km s$^{-1}$) and $R = 0.194$ (see Table A.1). A single excitation temperature was adopted, $T_{\rm ex} = 8$ K. The $H_2$ column density is computed assuming $T_{\rm dust} = T_{\rm ex}$. The CN fractional abundance $X({\rm CN}) = [{\rm CN}]/[{\rm H_2}]$ was computed assuming [$^{12}$CN]/[$^{13}$CN] = 68 (Milam et al. 2005). Error bars are 1$\sigma$.

| $\delta x, \delta y$ ″, ″ | $W$ mK km s$^{-1}$ | $N(^{13}{\rm CN})$ $10^{12}$cm$^{-2}$ | $S_{1.3\ {\rm mm}}$ MJy sr$^{-1}$ | $N({\rm H_2})$ $10^{22}$ cm$^{-2}$ | $X({\rm CN})$ $10^{-9}$ |
|---|---|---|---|---|---|
| –80, 80 | ≤25 | ≤0.1 | 4.1 ± 0.4 | 1.6 ± 0.1 | ≤0.5 |
| –60, 60 | 60 ± 15 | 0.3 ± 0.1 | 5.8 ± 0.6 | 2.3 ± 0.2 | 0.9 ± 0.2 |
| –40, 40 | 235 ± 30 | 1.2 ± 0.2 | 9.4 ± 0.4 | 3.6 ± 0.2 | 2.3 ± 0.3 |
| –20, 20 | 245 ± 20 | 1.3 ± 0.1 | 12.6 ± 0.8 | 4.9 ± 0.3 | 1.7 ± 0.2 |
| 0, 0 | 360 ± 80 | 1.8 ± 0.4 | 17.2 ± 0.5 | 6.6 ± 0.2 | 1.9 ± 0.4 |
| 20, –20 | 290 ± 75 | 1.5 ± 0.4 | 11.3 ± 1.1 | 4.4 ± 0.5 | 2.3 ± 0.7 |
| 40, –40 | 125 ± 20 | 0.6 ± 0.1 | 4.0 ± 0.6 | 1.6 ± 0.2 | 2.7 ± 0.6 |
| 60, –60 | ≤25 | ≤0.1 | 1.7 ± 0.5 | 0.7 ± 0.2 | ≤1.2 |
| 80, –80 | ≤25 | ≤0.1 | 0.5 ± 0.4 | 0.1 ± 0.1 | ≤5.8 |
| –40, –40 | ≤25 | ≤0.1 | 2.0 ± 0.3 | 0.8 ± 0.1 | ≤1.0 |
| –20, –20 | 190 ± 25 | 1.0 ± 0.1 | 7.0 ± 1.4 | 2.8 ± 0.5 | 2.3 ± 0.5 |
| 0, 0 | 360 ± 80 | 1.8 ± 0.4 | 17.2 ± 0.5 | 6.6 ± 0.2 | 1.9 ± 0.4 |
| 20, 20 | 110 ± 25 | 0.6 ± 0.1 | 9.2 ± 1.6 | 3.6 ± 0.6 | 1.1 ± 0.3 |
| 40, 40 | 60 ± 25 | 0.3 ± 0.1 | 3.0 ± 0.3 | 1.2 ± 0.1 | 1.8 ± 0.8 |

**Table 2.** $^{13}$CN(1–0) column density in L 183 (see Fig. 5). As Table 1, with the same excitation temperature, $T_{\rm ex} = 8$ K.

| $\delta x, \delta y$ ″, ″ | $W$ mK km s$^{-1}$ | $N(^{13}{\rm CN})$ $10^{12}$cm$^{-2}$ | $S_{1.3\ {\rm mm}}$ MJy sr$^{-1}$ | $N({\rm H_2})$ $10^{22}$ cm$^{-2}$ | $X({\rm CN})$ $10^{-9}$ |
|---|---|---|---|---|---|
| –40, 0 | ≤5 | ≤0.0 | 8.2 ± 1.1 | 3.3 ± 0.4 | ≤0.1 |
| –20, 0 | 125 ± 20 | 0.6 ± 0.1 | 15.8 ± 1.4 | 6.1 ± 0.6 | 0.7 ± 0.1 |
| 0, 0 | 165 ± 20 | 0.9 ± 0.1 | 18.3 ± 0.5 | 7.0 ± 0.2 | 0.8 ± 0.1 |
| 20, 0 | 75 ± 15 | 0.4 ± 0.1 | 12.2 ± 1.4 | 4.8 ± 0.6 | 0.5 ± 0.1 |
| 40, 0 | 130 ± 30 | 0.7 ± 0.1 | 7.1 ± 0.7 | 2.8 ± 0.3 | 1.6 ± 0.4 |
| 0, –40 | 85 ± 15 | 0.4 ± 0.1 | 9.8 ± 0.6 | 3.9 ± 0.2 | 0.7 ± 0.1 |
| 0, –20 | 105 ± 20 | 0.5 ± 0.1 | 14.2 ± 1.2 | 5.6 ± 0.5 | 0.7 ± 0.1 |
| 0, 0 | 165 ± 20 | 0.9 ± 0.1 | 18.3 ± 0.5 | 7.0 ± 0.2 | 0.8 ± 0.1 |
| 0, 20 | 150 ± 15 | 0.8 ± 0.1 | 16.1 ± 0.6 | 6.3 ± 0.2 | 0.8 ± 0.1 |
| 0, 40 | 135 ± 20 | 0.7 ± 0.1 | 14.5 ± 0.2 | 5.7 ± 0.1 | 0.8 ± 0.1 |

Subject to the above assumptions, we derive the column density of $^{13}$CN from the integrated intensity of the strongest hyperfine component at 108 780.201 MHz, which was taken to have a relative intensity $R = 0.194$ of the total (Bogey et al. 1984, and Table A.1). We used the formulation of A07. Our results are summarized in Tables 1 and 2 and shown in Fig. 5, where the error bars on the integrated intensity are $\sigma_{\rm T}\sqrt{FWHM \times \delta v}$.

From the continuum intensity at 1.3 mm, smoothed to the resolution of the $^{13}$CN(1–0) beam, we computed the $H_2$ column density as $N({\rm H_2}) = S_{1.3\ {\rm mm}}/(\kappa\mu m_{\rm H} B_\nu(T_{\rm dust}))$, where $\mu = 2.33$ is the mean molecular weight of the gas, $m_{\rm H}$ is the mass of atomic hydrogen and $\kappa = 0.01$ cm$^2$ g$^{-1}$ is the dust opacity per unit mass column density (Genzel 1992). The error bars are computed from the dispersion of the brightness inside the 22″ beam. The derived fractional abundances of $^{13}$CN, with respect to $H_2$ and at the dust peak, are $2.8 \times 10^{-11}$ and $1.3 \times 10^{-11}$ in L 1544 and L 183, respectively. These convert into CN fractional abundances of $1.9 \times 10^{-9}$ and $0.8 \times 10^{-9}$, assuming [$^{12}$CN]/[$^{13}$CN] = 68 (Milam et al. 2005).

From Fig. 5, we conclude that $^{13}$CN follows the dust and hence that the CN fractional abundance does not vary greatly with density in the centres of these cores; this is in sharp contrast to results for other species, in particular to observations of CO (Caselli et al. 1999) and NO (A07). It is also in contrast to the results of Tafalla et al. (2006), who found that, in L 1498

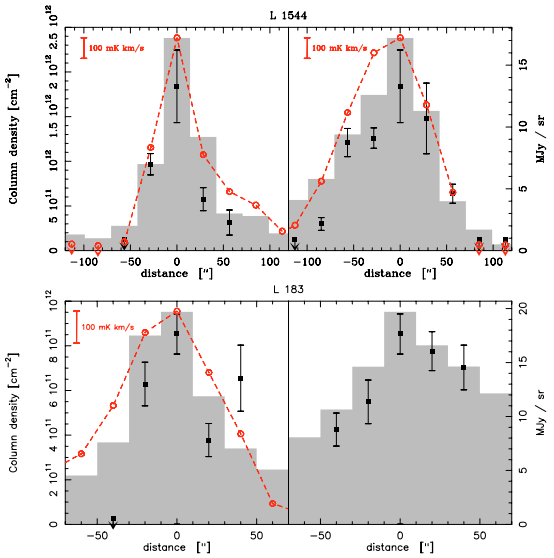


**Fig. 5.** Cuts through L 1544 (*top*) and L 183 (*bottom*). Filled squares: $^{13}$CN total column density (Tables 1 and 2) in cm$^{-2}$ (*left hand scale*). Open red circles: integrated intensity (in mK km s$^{-1}$: scale is indicated in top left corner) of the $(J, F_1, F) = 1, 0, 1 \rightarrow 0, 1, 2$ transition of $N_2H^+$ (see A07). Light histogram: dust emission in MJy sr$^{-1}$ (*right hand scale*).

and L 1517B, most C-containing molecules (though CN was not observed) deplete towards the density peaks in these objects. To our knowledge, CN is the first C-containing species which appears to avoid "depletion" towards the density peaks of prestellar cores, although more observations are required to confirm this general statement. The CN fractional abundances which we derive vary little with offset (and, by inference, with density), as Tables 1 and 2 show. In the case of L 183, they differ little also from the CN fractional abundances derived from observations with a larger beam and at various positions in the core (Dickens et al. 2000). We conclude that, even in situations where CO (the main sink of C) is highly depleted, some C-containing species can survive to densities of the order of to $10^6$ cm$^{-3}$.

## 4. Conclusions

The main conclusion of this work is that CN remains in the gas phase at densities close to $10^6$ cm$^{-3}$ in prestellar cores. This result is surprising, given that CO, which is the main repository of gas-phase carbon, is clearly depleted at such densities. It follows that CN can serve as a kinematic tracer of the high-density material. The profiles of $N_2H^+(1-0)$ from A07 and of $^{13}$CN from the present observations are in generally good agreement, suggesting that both molecules trace the same density regime. It is worth noting also that a double-Gaussian fit to the $^{13}$CN spectrum in L 1544 at offset $(-20, 20)$ yields one component with a velocity of $7.300 \pm 0.011$ km s$^{-1}$ and a *FWHM* of $0.130 \pm 0.025$ km s$^{-1}$. The associated upper limit on the kinetic temperature is $10.0 \pm 3.8$ K, which is in good agreement with the value from the best fit temperature profile of Crapsi et al. (2007) at a distance of 30″, where $T_{\rm kin} = 10$ K. In turn, this implies that the non-thermal linewidth is at most 0.65 times the thermal linewidth, and hence that turbulence has almost completely dissipated.

CN is important also as a possible tracer of the magnetic field in dense cores, by means of the Zeeman effect (Crutcher 1999). There exist already indirect estimates of the magnetic field in L 1544 and L 183, based upon the Chandrasekhar & Fermi (1953) method, which are of the order of 100 $\mu$G (Crutcher et al. 2004). Independent and direct measurements, based on the Zeeman effect, are highly desirable. In this context, we note that OH Zeeman measurements are sensitive only to the outer core, owing to the large beam size and to the depletion of oxygen towards the centre of the core.

The fact that CN is not depleted in the nuclei of L 1544 and L 183 has interesting consequences for the chemistry in these cores. One likely conclusion is that, although CO is depleted by more than an order of magnitude at densities of a few times $10^5$ to $10^6$ cm$^{-3}$, there remains sufficient CO in the gas phase to supply carbon to other, less abundant species. Quantifying this statement will require model calculations, which are under way. An expectation which is based on the model calculations is that the effective [C]/[O] gas-phase abundance ratio in dense depleted regions, such as those in L 1544 and L 183, is larger than the value of [C]/[O] = 0.67 adopted by Flower et al. (2005). The [CN]/[NO] abundance ratio is sensitive to the amount of free oxygen (i.e. not tied up in CO) in the gas phase. Our observations of L 1544 establish a lower limit to [CN]/[NO] of order 0.1 in the high density region; this suggests a [C]/[O] of at least 0.8. There will be consequences for HCN and HNC, and it would be useful to determine limits on the abundances of these species in the dense cores of L 1544 and L 183. We note that our suggestion (A07) that CN acts as an intermediary in the nitrogen chemistry is supported by the present results.

*Acknowledgements.* We are indebted to the referee for some helpful and perceptive comments on the original version of this letter.

## References

Akyilmaz, M., Flower, D. R., Hily-Blant, P., Pineau des Forêts, G., & Walmsley, C. M. 2007, A&A, 462, 221 (A07)
Belloche, A., & André, P. 2004, A&A, 419, L35
Bergin, E. A., Alves, J., Huard, T., & Lada, C. J. 2002, ApJ, 570, L101
Bogey, M., Demuynck, C., & Destombes, J. L. 1984, Can. J. Phys., 62, 1248
Caselli, P., Walmsley, C. M., Tafalla, M., Dore, L., & Myers, P. C. 1999, ApJ, 523, L165
Chandrasekhar, S., & Fermi, E. 1953, ApJ, 118, 113
Crapsi, A., Caselli, P., Walmsley, M. C., & Tafalla, M. 2007, A&A, 470, 221
Crutcher, R. M. 1999, ApJ, 520, 706
Crutcher, R. M., Nutter, D. J., Ward-Thompson, D., & Kirk, J. M. 2004, ApJ, 600, 279
Dickens, J. E., Irvine, W. M., Snell, R. L., et al. 2000, ApJ, 542, 870
Flower, D. R., Pineau des Forêts, G., & Walmsley, C. M. 2005, A&A, 436, 933
Genzel, R. 1992, in Saas-Fee Advanced Course 21: The Galactic Interstellar Medium, ed. W. B. Burton, B. G. Elmegreen, & R. Genzel, 275
Gerin, M., Combes, F., Encrenaz, P., et al. 1984, A&A, 136, L17
Hily-Blant, P., Pety, J., & Guilloteau, S. 2005, CLASS evolution: I. Improved OTF support, Tech. rep., IRAM
Leger, A., Jura, M., & Omont, A. 1985, A&A, 144, 147
Milam, S. N., Savage, C., Brewster, M. A., Ziurys, L. M., & Wyckoff, S. 2005, ApJ, 634, 1126
Öberg, K. I., van Broekhuizen, F., Fraser, H. J., et al. 2005, ApJ, 621, L33
Pagani, L., Bacmann, A., Motte, F., et al. 2004, A&A, 417, 605
Pagani, L., Bacmann, A., Cabrit, S., & Vastel, C. 2007, A&A, 467, 179
Pety, J. 2005, in SF2A-2005: Semaine de l'Astrophysique Francaise, ed. F. Casoli, T. Contini, J. M. Hameury, & L. Pagani, 721
Pineau des Forêts, G., Roueff, E., & Flower, D. R. 1990, MNRAS, 244, 668
Tafalla, M., Myers, P. C., Caselli, P., Walmsley, C. M., & Comito, C. 2002, ApJ, 569, 815
Tafalla, M., Santiago-García, J., Myers, P. C., et al. 2006, A&A, 455, 577
van der Tak, F. F. S., Caselli, P., & Ceccarelli, C. 2005, A&A, 439, 195
Ward-Thompson, D., Motte, F., & André, P. 1999, MNRAS, 305, 143
Williams, J. P., Myers, P. C., Wilner, D. J., & di Francesco, J. 1999, ApJ, 513, L61

**Table A.1.** Hyperfine structure components of the $(N' \rightarrow N) = 1 \rightarrow 0$ transitions in $^{13}$CN. $S$ is the line strength, and the relative intensities ($R$) are normalized to the sum of all the components. The selection rules are $\Delta F_1 = 0, \Delta F_2 = 0, \pm 1$ and $\Delta F = 0, \pm 1$ (Bogey et al. 1984).

| $F_1$ | $F_2 \rightarrow F_2'$ | $F \rightarrow F'$ | Frequency MHz | $S(F,F')$ | $R$ |
|---|---|---|---|---|---|
| 0 | $1 \rightarrow 0$ | $2 \rightarrow 1$ | 108 651.2970 | 1.667 | 0.139 |
| | | $1 \rightarrow 1$ | 108 636.9230 | 1.000 | 0.083 |
| | | $0 \rightarrow 1$ | 108 631.1210 | 0.333 | 0.028 |
| 1 | $2 \rightarrow 1$ | $1 \rightarrow 0$ | 108 786.9820 | 0.556 | 0.046 |
| | | $2 \rightarrow 1$ | 108 782.3740 | 1.250 | 0.104 |
| | | $3 \rightarrow 2$ | 108 780.2010 | 2.333 | 0.194 |
| | | $1 \rightarrow 1$ | 108 793.7530 | 0.417 | 0.035 |
| | | $2 \rightarrow 2$ | 108 796.4000 | 0.417 | 0.035 |
| | | $1 \rightarrow 2$ | 108 807.7879 | 0.028 | 0.002 |
| 1 | $1 \rightarrow 1$ | $1 \rightarrow 0$ | 108 638.2120 | 0.333 | 0.028 |
| | | $2 \rightarrow 1$ | 108 643.5900 | 0.417 | 0.035 |
| | | $1 \rightarrow 1$ | 108 645.0640 | 0.250 | 0.021 |
| | | $2 \rightarrow 2$ | 108 657.6460 | 1.250 | 0.104 |
| | | $0 \rightarrow 1$ | 108 645.0640 | 0.333 | 0.028 |
| | | $1 \rightarrow 2$ | 108 658.9480 | 0.417 | 0.035 |
| 1 | $0 \rightarrow 1$ | $1 \rightarrow 0$ | 108 406.0905 | 0.111 | 0.009 |
| | | $1 \rightarrow 1$ | 108 412.8620 | 0.333 | 0.028 |
| | | $1 \rightarrow 2$ | 108 426.8890 | 0.556 | 0.046 |

**Table B.1.** Integrated intensities of the CN($N = 1 \rightarrow 0, F_2 = 3/2 \rightarrow 1/2$) HFS components, relative to the $F = 5/2 \rightarrow 3/2$ line, towards the (0, 0) positions in L 183 and L 1544. The observed values of $\tilde{I}$ are compared to the optically thin LTE prediction (Savage et al. 2002).

| $F \rightarrow F'$ | Frequency MHz | $\tilde{I}$ L 183 | $\tilde{I}$ L 1544 | LTE |
|---|---|---|---|---|
| $1/2 \rightarrow 3/2$ | 113 520.414 | $5.1 \pm 1.2$ | $0.8 \pm 0.1$ | 0.037 |
| $3/2 \rightarrow 3/2$ | 113 508.934 | $7.4 \pm 1.7$ | $0.9 \pm 0.1$ | 0.296 |
| $1/2 \rightarrow 1/2$ | 113 499.643 | $5.8 \pm 1.3$ | $0.7 \pm 0.1$ | 0.296 |
| $5/2 \rightarrow 3/2$ | 113 490.985 | 1 | 1 | 1 |
| $3/2 \rightarrow 1/2$ | 113 488.142 | $5.2 \pm 1.2$ | $0.9 \pm 0.0$ | 0.371 |

## Appendix A: Spectroscopic data

Table A.1 gives the strengths and relative intensities, $R$, of the 18 hyperfine components of the $N = 1{-}0$ transition of $^{13}$CN. The relative intensities are such that the sum over all components is unity. The two weakest hyperfine components [$F_1 = 1$, $(F_2 \rightarrow F_2') = (2 \rightarrow 1)$, $(F \rightarrow F') = (1 \rightarrow 2)$ and $(F_2 \rightarrow F_2') = (0 \rightarrow 1)$, $(F \rightarrow F') = (1 \rightarrow 0)$], which were omitted by Bogey et al. (1984), are included here. We note that the angular momentum coupling scheme is $\boldsymbol{S} + \boldsymbol{I}_1 = \boldsymbol{F}_1$, $\boldsymbol{F}_1 + \boldsymbol{N} = \boldsymbol{F}_2$, and $\boldsymbol{F}_2 + \boldsymbol{I}_2 = \boldsymbol{F}$, where $S = 1/2 = I_1$ and $I_2 = 1$; $S$ is the resultant electron spin quantum number, $N$ is the nuclear rotation quantum number, and $I_1$, $I_2$ are the nuclear spin quantum numbers of $^{13}$C and $^{14}$N, respectively (in the case of $^{12}$C, $I_1 = 0$).

## Appendix B: Observed line ratios

The relative integrated intensities of the observed HFS components have been computed at the $(0, 0)$ positions in both L 183 and L 1544 and compared with the values expected in the optically thin limit, under the assumption of LTE. These results are listed in Tables B.1 and B.2.

**Table B.2.** As Table B.1 for the $^{13}$CN($N = 1 \rightarrow 0, F_2 = 2 \rightarrow 1$) HFS components, relative to the $F = 3 \rightarrow 2$ component.

| $F \rightarrow F'$ | Frequency MHz | $\tilde{I}$ L 183 | $\tilde{I}$ L 1544 | LTE |
|---|---|---|---|---|
| $3 \rightarrow 2$ | 108780.2010 | 1 | 1 | 1 |
| $2 \rightarrow 1$ | 108782.3740 | $0.40 \pm 0.10$ | $0.65 \pm 0.15$ | 0.536 |
| $1 \rightarrow 0$ | 108786.9820 | $0.30 \pm 0.10$ | $0.35 \pm 0.15$ | 0.238 |
| $1 \rightarrow 1$ | 108793.7530 | $0.25 \pm 0.12$ | $\leq 0.40$ | 0.179 |
| $2 \rightarrow 2$ | 108796.4000 | $\leq 0.10$ | $\leq 0.30$ | 0.179 |

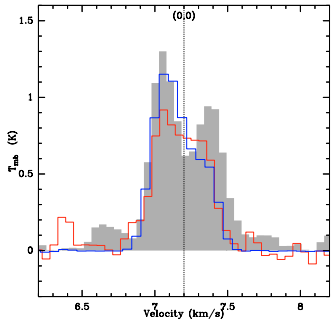


**Fig. C.1.** Comparison of line profiles towards L 1544 at offsets (0, 0). CN: weakest HFS component at 113 520.4315 MHz (shaded histogram). $^{13}$CN: HFS component at 108 780.2010 MHz, multiplied by 7 (red histogram). $N_2H^+$: HFS component at 93 176.2650 MHz, multiplied by 0.5 (blue histogram, from A07). The dashed line indicates the LSR velocity of 7.2 km s$^{-1}$.

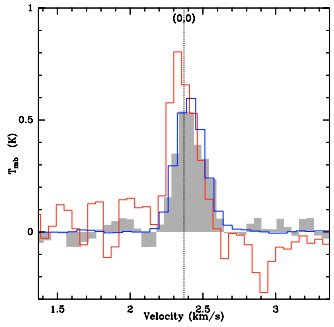


**Fig. C.2.** As Fig. C.1, but towards L 183. The HFS component at 93 176.2650 MHz of $N_2H^+$ is multiplied by 0.25 (blue histogram, from A07). The dashed line indicates the LSR velocity of 2.37 km s$^{-1}$.

## Appendix C: Line profiles

Figures C.1 and C.2 show the profiles of the different tracers observed towards L 1544 and L 183, respectively. The $N_2H^+$ data are taken from A07. In L 1544, at those positions where the line is double-peaked, all the profiles are mutually consistent, except possibly at offset $(-20, -20)$, where only the CN HFS component shows two velocity components (but the signal-to-noise ratio of the $^{13}$CN line is too low to draw a definite conclusion). In L 183, all lines are consistent at all positions.